Accepted Manuscript

Influence of High Fidelity Structural Models on the Predicted Mass of Aircraft Wing Using Design Optimization

Odeh Dababneha, Timoleon Kipouros

Please cite this article in press as: O. Dababneha, T. Kipouros, Influence of High Fidelity Structural Models on the Predicted Mass of Aircraft Wing Using Design Optimization, *Aerosp. Sci. Technol.* (2018), https://doi.org/10.1016/j.ast.2018.05.043

1
2
Influence of High Fidelity Structural Models on the Predicted Mass of Aircraft Wing Using Design Optimization

3 Odeh Dababneh[a]*, Timoleon Kipouros[b,c]

4 *School of Mechanical and Aerospace Engineering, Queen's University Belfast,*
5 *Belfast, Northern Ireland BT9 5AH, United Kingdom*

6 *bEngineering Design Centre, Department of Engineering*
7 *University of Cambridge, Cambridge, CB2 1PZ, United Kingdom*

8 *cSchool of Aerospace, Transport and Manufacturing*
9 *Cranfield University, Cranfield, MK43 0AL, United Kingdom*

10

11 **Abstract**

12 This paper explores the necessary and appropriate level of detail that is required to describe the structural

13 geometry of aircraft wings accurately enough to predict the mass of the main load-carrying wing structure

14 to an acceptable level of accuracy. Four different models of increasing structural fidelity are used to

15 describe the wingbox structure of a realistic real-world aircraft wing. The wingbox of the NASA

16 Common Research Model served as a test model for exploring and analyzing the trade-off between the

17 granularity level of the wingbox geometry description under consideration and the computational

18 resources necessary to achieve the required degree of accuracy. The mass of metallic and composite

19 wingbox configurations was calculated via finite element analysis and design optimization techniques.

20 The results provided an insight into the competence of certain wingbox models in predicting the mass of

21 the metallic and composite primary wing structures to an acceptable level of accuracy, and in

22 demonstrating the relative merits of the wingbox structural complexity and the computational time and

23 input efforts for achieving the required level of accuracy.

24 **Keywords:** Wing Mass; Primary Wing Structures; High-Fidelity Models; Finite Element; Optimization

25 **Nomenclature**

26 $a_{composite}$ Cross-sectional area of the composite wingbox flanges, mm^2

27 $a_{metallic}$ Cross-sectional area of the metallic wingbox flanges, mm^2

28 b Wing semi-span, m

29 C Wing chord length, m

30 E_{11} Longitudinal modulus, GPa

31 E_{12} Transverse modulus, GPa

32 E Elastic modulus, GPa

33 EI   Bending stiffness

34 FI Failure index

35 _____

36 *Corresponding author
37 *E-mail address:odeh.da@gmail.com; o.dababneh@qub.ac.uk*

1

| 38 | G_{12} | In-plane shear modulus, GPa |
39	GJ	Torsional stiffness
40	$M(x)$	Objective function representing the wingbox structural mass
41	n_{ply}	Number of plies
42	$t_{metallic}$	Thickness of the metallic wingbox panels, mm
43	$\delta_{tip(Z)}$	Z-Component of the wingtip displacement
44	$(\delta)_{max}^+$	Maximum vertical displacement in positive direction
45	$(\delta)_{max}^-$	Maximum vertical displacement in negative direction
46	$\varepsilon_{allowable}$	Allowable strain
47	$\varepsilon_{principal}$	Principal strain
48	Θ_{tip}	Angle of twist at the wingtip, deg
49	$\mu\varepsilon$	Micro strain
50	ν_{12}	Major Poisson's ratio
51	$\sigma_{allowable}$	Allowable stress
52	$\sigma_{von\,Mises}$	von Mises stress
53	$\sigma_{ultimate}$	Ultimate stress
54	σ_{axial}	Axial stress

1. Introduction

56   In a conventional approach to aircraft wing mass estimation at the early stages of the design process,
57   wing mass property design engineers usually follow a particular published methodology, such as one of
58   those proposed by Raymer [1], Roskam [2] or Torenbeek [3]. Taking up as much as 35-50% of the
59   operating empty weight of modern transport aircraft [4], the wing is one of the heaviest structural
60   components of an aircraft. In recent years, aircraft manufacturers and research institutes have been
61   focusing on aircraft concepts that require new wing designs. The NASA Common Research Model
62   (CRM) for a generic transport aircraft model is an example [5,6]. The design of an efficient aircraft wing
63   featuring new technologies has always represented a substantial challenge for aircraft designers,
64   especially when the proposed novel concept challenges the existing knowledge base and the accuracy of
65   normally used empirical methods and statistical data collected from previously constructed aircraft. These
66   methods are generally limited to conventional aircraft designs constructed from light metallic alloys and
67   are unable to assess the relative benefits of novel wing design concepts as well as advanced materials,
68   such as composite materials. In the literature, great efforts have been put into and reported on developing
69   and classifying wing mass prediction methods [7-10]. This is because of the well-defined structural role
70   of the wingbox as a primary load-carrying component and the importance of optimum wing design as a
71   significant subject of the preliminary design phase [11]. The open literature on the subject of wing mass
72   estimation methods and their applications in the aerospace industry has been comprehensively discussed
73   by Dababneh and Kipouros in [12]. In their work, the current state of the art of aircraft wing mass
74   estimation methods has been reviewed. Special attention has been given to classifications of wing mass

75   estimation methods and to the current challenges and technological difficulties in wing mass estimation

76   methods. According to [12], determining the mass of an aircraft wing, for which the database is

77   insufficient or non-existent or the wing design lies beyond the use of empirical methods, via fully

78   integrated finite element analysis [13-17], and design optimization methods [18,19,20] appears to be a

79   promising approach to consider at the early stages of the design process. This has been made possible

80   over the last 10 years by the increased processing power of computers, the advancements in computer-

81   aided design, the enhancement of multi-dimensional design space visualizations, simultaneous

82   calculation, visual screening and representations of a variety of design analysis and optimization results

83   [21]. With design optimization, one is usually concerned with the chosen form of the structural model and

84   the finite element level of detail in the wingbox that is needed to be considered in order to achieve the

85   required results. Ciampa et al. [22] highlighted the importance of significantly reduced complexity finite

86   element models in the pre-design phase process of aircraft wing structures. In their work, they showed

87   that the wing skin stiffened panels can be represented by stiffness-equivalent panels. This procedure

88   enables a fast search for an optimum mass with low computational resources, but does not provide

89   enough information for the sizing of stiffened panels. In another example, Yang et al. [23], revealed that

90   adequate natural frequency and mode shape results for a complex wing structure can be achieved by using

91   an equivalent wing model, in which each wing segment is modeled as equivalent plate, reducing the wing

92   structural complexity to a simple model and hence the cost of the design task. In the field of structural

93   design optimization concepts for aerospace industry, Ritter [24] showed that while the industry-standard

94   beam-rod representation of aircraft wing is sufficient for linear aeroelastic simulations, a 3D wingbox

95   model, which resembles a real aircraft wing much more realistically, will provide valuable insight into the

96   aeroelastic dynamic behavior of the structure especially when the design optimization process is focused

97   on aeroelastic tailoring [25]. The scope of this study is to investigate and understand the effect of using

98   different wingbox configurations of increasing structural complexity on the mass estimation of the wing

99   primary structure. The goals of the present study are mainly twofold. The first is to identify and select an

100   appropriate model that can predict the mass of the CRM wingbox to an acceptable level of accuracy. It

101   also has to allow the designer to explore and asses the design decisions made, such as the choice of

102   construction material, at an early stage of the design process, thus eliminating any costly changes during

103   the detailed design process, and can serve as well as a baseline model for future complex structural

104   optimization studies. The second is to demonstrate the trade-off between the wingbox structural

105   complexity models under consideration and the user input efforts and computational time needed to

106   achieve sufficiently accurate results for the intended design and analysis purposes.

107   **2.   Technical description of the CRM wing**

108   The CRM is a modern single-aisle transport-class aircraft configuration that was generated as an open

109   geometry for collaborative research within the aerodynamics community. It has a wingspan of 58.76 m, a

110   mean aerodynamic chord of 7.0 m, an aspect ratio of 9.0, a taper ratio of 0.275, a leading edge sweep

111   angle of 35°, a break along the trailing edge at 37% of the semi-span (also referred to as the yehudi

112   break), a wing tip chord of 2.73 m, a wing root chord of 13.56 m and a cruise Mach number of 0.85. The

113   maximum take-off mass (MTOM) is set to 260,000 kg. The maximum cruise speed limit is set to $V_C =$

114   193 m/s EAS with a cruise Mach number of $M_C = 0.85$. The dive speed is set to $V_D = 221.7$ m/s EAS with

115   a dive Mach number of $M_D = 0.92$, which results from the equation $M_D = M_C + 0.07$ given in [26]. The

116   cruise altitude is taken as 10,668 m. The planform of the wing and the relevant data are presented in Fig.

117   2.

118

119

120

121

122

123

124

125

126

127

128
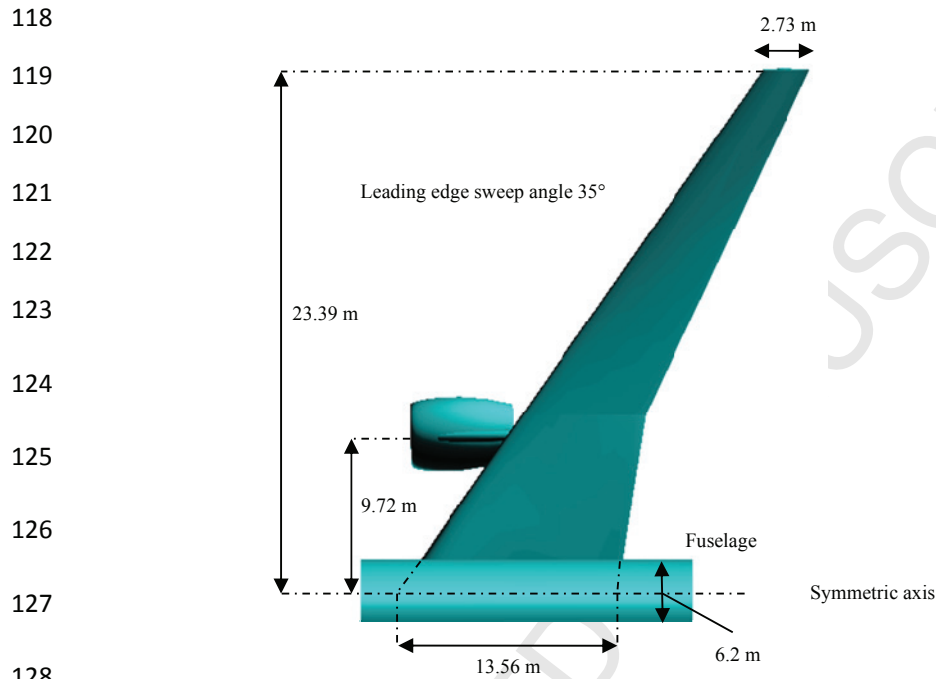
129   **Fig. 2** Planform of the CRM wing

130   **3.**   **Structural and finite element modeling of the CRM wing**

131   The CRM primary wing structure is modeled to meet the minimum design requirements set forth in

132   the Federal Aviation Regulations (FAR) Part 25 [27] and/or the European Aviation Safety Agency

133   (EASA) CS-25 [26]. Traditional two-spar wingbox architecture is used as a baseline design. The external

134   geometry is defined by CRM.65-BTE airfoil sections and the wingbox is derived from the wing surface

135   model by defining the front and rear spar positions at 12% and 71% of the local airfoil chord. The internal

136   layout is defined by the stiffener pitch, rib pitch and orientation based on the values for a typical large

137   transport aircraft wing. Fig. 3 shows the CRM wing surface model and the wingbox derived from it.

138

139

140

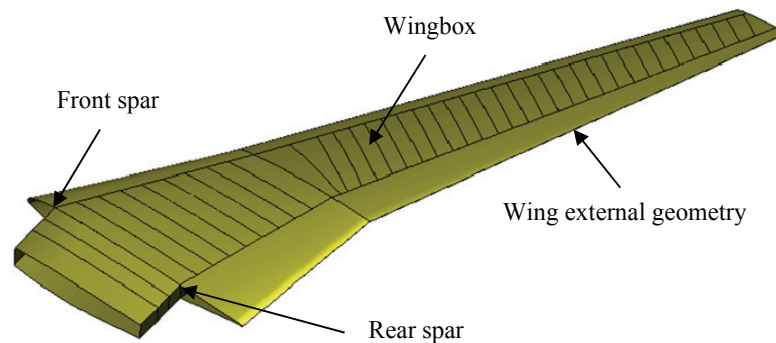141

142

143

144

145

146

147

148

149

150

151   **Fig. 3** Surface and wingbox model of the CRM wing

152   **3.1   Description of the considered structural models**

153   The main load carrying wing structure is created using different models of increasing structural

154 fidelity, as shown in Figs. 4-7. The main goal is to identify and select an appropriate model that can

155 predict the mass of the primary wing structure to an acceptable level of accuracy. This done by

156 conducting comparative effectiveness studies that aim to investigate the effects of using different

157 wingbox configurations on the definition of the analysis and optimization models, and therefore on the

158 wingbox mass estimation.

159   **1. Wingbox section model 1**

160   In this model, as shown in Fig. 4, each bay in the wingbox is modeled by four un-stiffened thin-walled

161 panels. These panels represent the upper and lower skins of the wingbox, as well as the front and rear spar

162 webs. The thicknesses of the panels are treated as independent design variables representing the wing

163 torsion box and contributing to bending strength properties.

164   t_1, skin_upp

165

166   t_3, web_front t_4, web_rear

167

168   t_2, skin_low
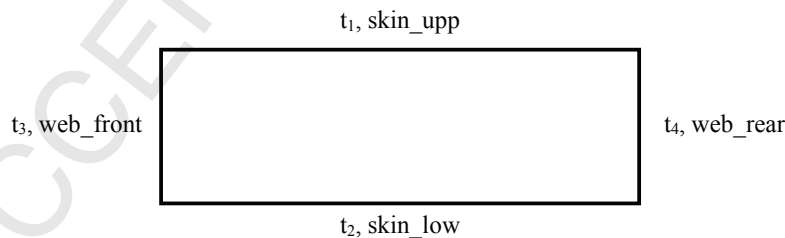
169   **Fig. 4** Wingbox section Model 1 and related design parameters

170   **2. Wingbox section model 2**

171   This model, as shown in Fig. 5, retraces the previous one and considers the rib thickness as a fifth

172 independent design variable. The number of ribs and their spacing is determined from previously acquired

173 knowledge and evidence from other engineering designs. The ribs and their spacing must maintain the

174 aerodynamic shape of the wing and provide enough clearance through the access hole between each rib

175 section for inspections and maintenance throughout the operational life of the aircraft. A better evaluation

176 and understanding of the wingbox in-plane and out-of-plane stiffness and bending requirements is hoped
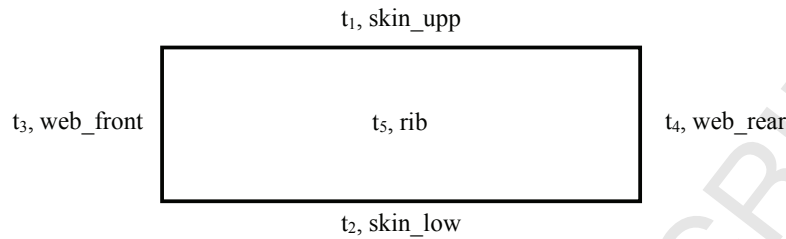
177 to be gained using this model.

178

t_1, skin_upp

179

180 t_3, web_front $\qquad$ t_5, rib $\qquad$ t_4, web_rear

181

182 t_2, skin_low

183 **Fig. 5** Wingbox section Model 2 and related design parameters

184 **3. Wingbox section model 3**

185 Four additional independent design variables are added to the third model: upper and lower spar caps

186 are added to the front and rear spars, as illustrated in Fig. 6. The spar caps take most of the loads from the

187 bending moments, and due to the presence of the spar web, one cap experiences a tension force while

188 another undergoes compression. The spar caps' cross-sectional areas are usually large and vary along the

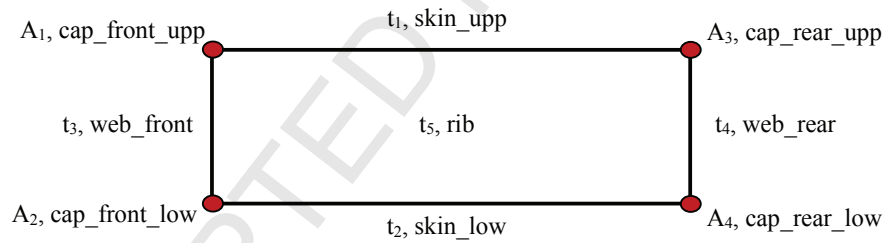189 wing.

190 A_1, cap_front_upp $\qquad$ t_1, skin_upp $\qquad$ A_3, cap_rear_upp

191

192 t_3, web_front $\qquad$ t_5, rib $\qquad$ t_4, web_rear

193

194 A_2, cap_front_low $\qquad$ t_2, skin_low $\qquad$ A_4, cap_rear_low

195 **Fig. 6** Wingbox section Model 3 and related design parameters

196 **4. Wingbox section model 4**

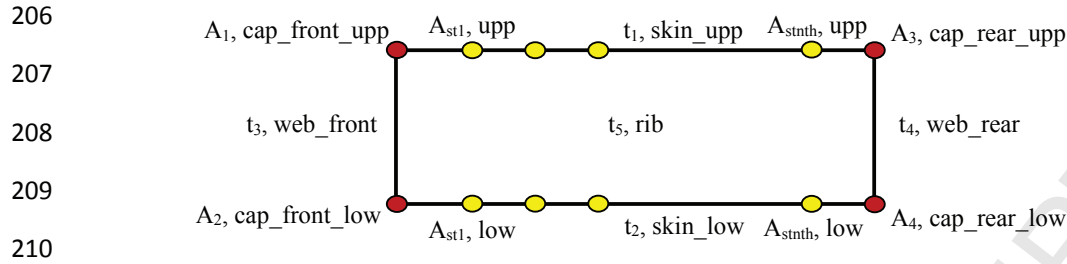197 Stiffeners are added as new independent design variables to the previous model, as shown in Fig. 6.

198 They are used to support the skin between the ribs and to account for the instability of the thin-walled

199 panels. The stiffeners are also used to resist the part of the bending moment which is not resisted by the

200 spar caps and to take some of the tension and compression loads with effective skin areas. The number of

201 stiffeners and the distance between them is determined from previous design experience.

202

203

204

205

6

A_1, cap_front_upp $\quad A_{st1}$, upp $\quad t_1$, skin_upp $\quad A_{stnth}$, upp $\quad A_3$, cap_rear_upp

t_3, web_front $\qquad\qquad t_5$, rib $\qquad\qquad t_4$, web_rear

A_2, cap_front_low $\quad A_{st1}$, low $\quad t_2$, skin_low $\quad A_{stnth}$, low $\quad A_4$, cap_rear_low

Fig. 7 Wingbox section Model 4 and related design parameters

The wingbox of the CRM aircraft is designed by considering both metallic and composite materials, which have a high strength-to-weight ratio for lightweight structures, high strength and stiffness properties, good fatigue and corrosion resistance. High-strength aluminum 7050-T7451 alloy [28] is used for the design of the upper skins, upper stringers and spar caps of the wingbox, and 2024-T351 alloy [29] is used for the design of the lower skins, lower stringers and the ribs, since it is better suited for structures stressed by cyclic tension loads and therefore prone to fatigue damage. In addition to aluminium alloys, composite materials made up of T300 carbon fibres and N5208 epoxy resin, which is widely used in the aircraft industry, is used as a second material choice for the wingbox structure design [30]. For modeling the wingbox using a composite material, a symmetric and balanced laminate with ply orientation angles of [45/0/-45/90]s was created in order to get an orthotropic material. The aim of this design procedure was to avoid shear extension and membrane bending coupled behaviors.

3.2 Aerodynamic loads calculation of the CRM wing

For the CRM wing, the design loads are obtained from two scenarios, related to flight maneuvers and gust conditions, in accordance with the standard airworthiness certification regulations [26,27]:

1. Symmetric pull-up maneuver load for the maximum positive limit load factor at maximum take-off mass and maximum dive speed, V_D, at sea-level standard atmospheric conditions;

2. Gust loads for the maximum gust load factor at maximum zero fuel mass and maximum cruise speed, V_C, at a critical gust altitude of 6,100 m.

The symmetric pull-up maneuver at the limit load factor ($n = 2.5$) at maximum take-off mass (260,000 kg) and design dive speed ($V_D = 221.7$ m/s EAS, $M_D = 0.65$) at sea-level conditions was found to be the critical one for the design, analysis and sizing optimization of the CRM wingbox and hence the mass estimation. There are currently several theoretical methods available for determining the aerodynamic loading of an aircraft wing. Many of the theoretical solutions have been programmed for digital computation, and separate computer programs have been used to calculate the aerodynamic forces on an aircraft wing in different flow conditions. The choice of the appropriate method depends on the complexity of the aircraft wing, the purpose of the analysis, the computational cost and the level of accuracy required at the design stage. In the current study, the spanwise lift force and pitching moment were calculated using the ESDU 95010 computer program. ESDUpac A9510 utilizes steady lifting-surface theory based on the Multhopp-Richardson solution to calculate the spanwise loading of wings

241 with camber and twist in subsonic attached flow [31]. Figs. 8 and 9 give the local overall lift and pitching

242 moment coefficients calculated about a local quarter chord.

243

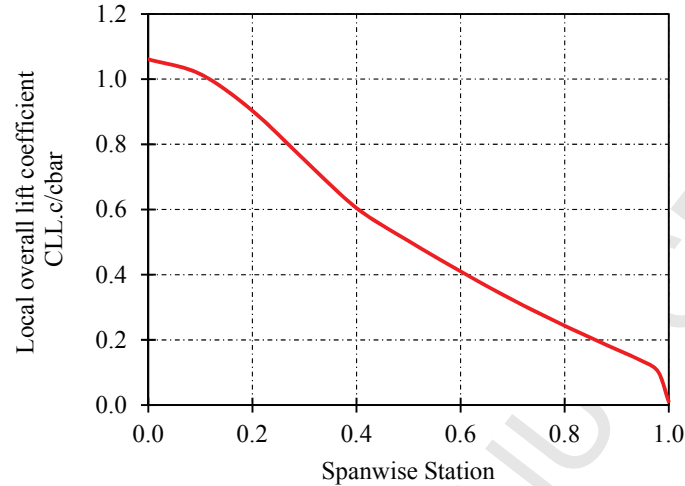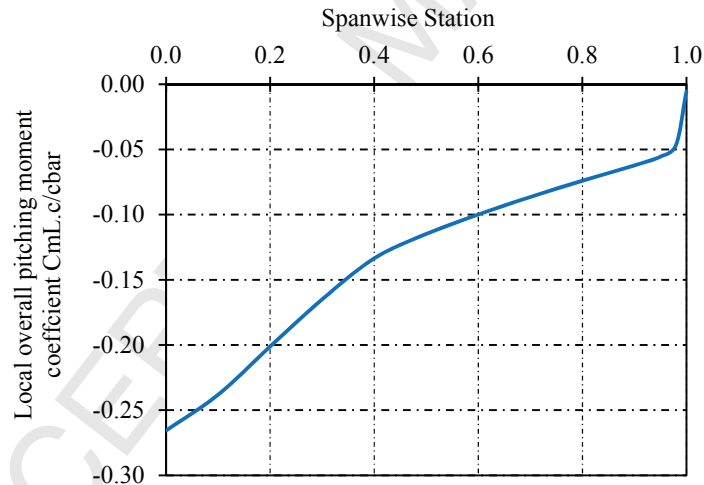**Fig. 8** Spanwise local overall lift coefficient

Fig. 9 Spanwise local overall pitching moment coefficient

3.3   Finite element modeling of the CRM wing

266   In the current study, the thin-walled structures of the CRM wingbox configurations (skins, webs and

267 ribs) were modeled using two-dimensional quadrilateral and triangular shell elements (CQUAD4,

268 CTRAI3) with in-plane membrane and bending stiffness. On the other hand, stringers and spar caps were

269 modeled using one-dimensional rod elements (CROD) with axial stiffness. Finite element models of the

270 CRM wingbox configurations are generated using MSC Patran, based on the physical dimensions and

271 material properties of the structural cross-sectional models as specified in section 3 The wing planform

8

272 was modeled for a half-wing section. The structure within the leading and trailing edges was not modeled

273 and the lower skin of the wing has no manholes. Fig. 10 shows the finite element mesh models for the

274 CRM wingbox structures.

Model 1

Model 2
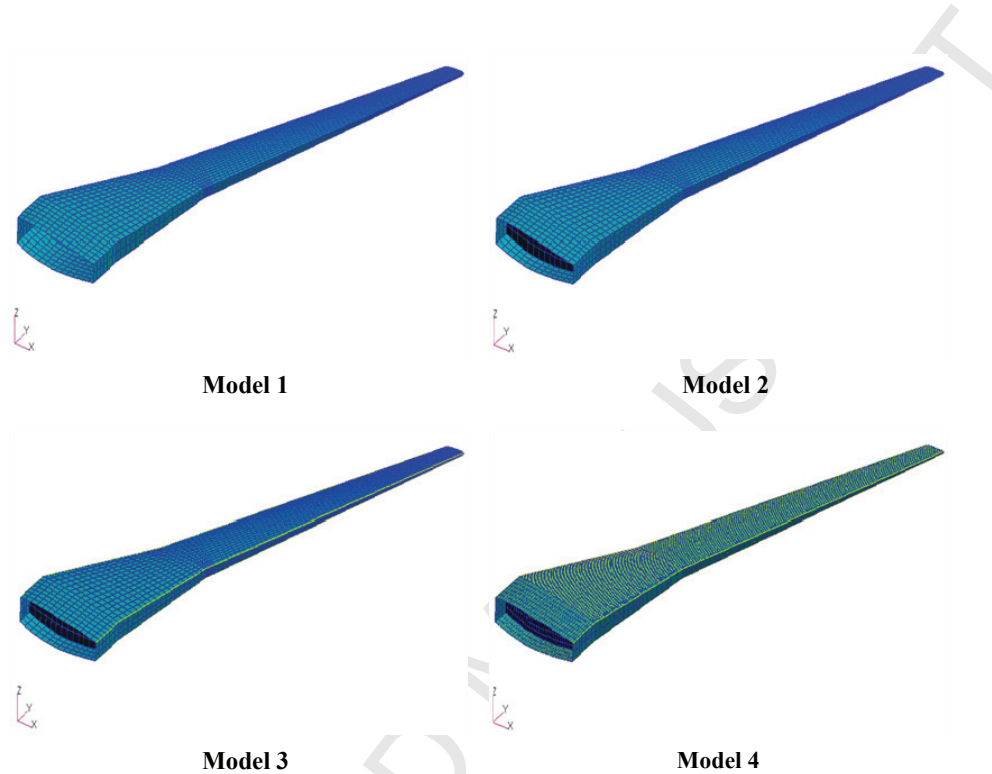
Model 3

Model 4

275

276 **Fig. 11** Finite element mesh models of the CRM wingbox structures-Models 1-4

277 The aerodynamic loads were discretely distributed along the wing by computing the equivalent lift force

278 and pitching moment components at rib boundary locations at 25% of the local chord length. They were

279 introduced to the wingbox finite element model by means of multipoint constraint (MPC) non-stiffening

280 rigid body elements (RBE3) in the rib's perimeter nodes. Spring elements (CEALS1) combined with

281 RBE2 elements were used to create realistic boundary conditions at the wingbox root at the aircraft

282 centerline. The spring elements were attached to a fixed ground point. The translational and rotational

283 stiffness properties were selected to result in end boundary conditions sufficiently close to the clamped

284 case, due to the lack of available data on wingbox root stiffness values for real aircraft structures in the

285 open literature. The wingbox finite element models have been verified by numerous quality pre-analysis

286 checks, including element free edge, mesh and element quality, boundary conditions, coincident nodes,

287 material and element properties, and element normal. Finite element model checks help to safeguard

288 against fundamental errors, and also guard against the frustration associated with having the solver run for

289 a considerable amount of time, only to abort due to incorrect or missing data.

4.   Structural design optimization of the CRM wingbox

Structural optimization methods evolved in the aerospace industry in the late 1950s, when the need to design lightweight structures was critical [32,33,34]. Since then, the aerospace manufacturing industry has shown increasing interest in the application of optimization methods for the optimum design of minimum-weight aircraft structural components [35,36,37]. The survey paper by Venkayya [38] presents an exhaustive review of relevant literature on the structural optimization of aerospace structures. In their work Wang et al. [39] offer numerous and important references on the applications of design optimization approaches to the field of aerospace structure engineering. The CRM wingbox structural optimization that is presented in this work purposely deals with property optimization. Therefore, the locations of the ribs, stiffeners and spars are considered invariable and shape optimization is not performed in this study. The optimization is performed using the commercially available off-the-shelf MSC Nastran gradient-based Sol 200 optimizer [40] which is widely used and recognized by the aerospace industry across the globe. One of the key advantages underlying the selection of gradient-based algorithms is their effectiveness in solving optimization problems where the design space is significantly large, and where the number of design variables is therefore considerably greater than the number of objectives and constraints. Another advantage is their relative computational efficiency due to rapid convergence rates with clear convergence criteria. However, one of the main drawbacks of gradient-based methods is the presence of multiple local optima, resulting in solutions where global optimality cannot be easily guaranteed. In gradient-based methods, global optimality is sought by randomly searching the design space from different starting points. In practice, one normally seeks procedures through which the design search space is explored in a cost-effective manner, aiming for a better optimal solution within an acceptable level of accuracy depending on the size and nature of the optimization problem. For this reason a practical design optimization procedure using gradient-based methods was utilized for the structural sizing for both metallic and composite configuration in order to calculate the mass of the CRM primary wing structure in an effective and efficient way. The reader may wish to refer to the work of Dababneh et al. [41] for more details regarding the practical design optimization framework.

4.1   Structural layout of the CRM wingbox models used for structural optimization

The load-carrying structure of NASA's Common Research Model transport aircraft wing configuration is used for the optimization. Four different wingbox models of increasing structural complexity were created as part of this study. The structural layout of the CRM wingbox models is given in Fig. 11. These models are discretized into components which act as design optimization zones along the span. These areas include the upper and lower skins, front and rear spar webs, ribs, spar caps and stiffeners. Model 1 contains 168 design zones. Model 2 contains 210 design zones. Model 3 contains 378 design zones. Model 4 contains 1,870 design zones. The chordwise design zones are prescribed by the stringer pitch, while in the spanwise direction the design zones are limited by the rib spacing. In the finite element model, each design field consists of a number of finite elements that all comprise the same thicknesses/cross-sectional areas and stiffness properties.

327

328

329
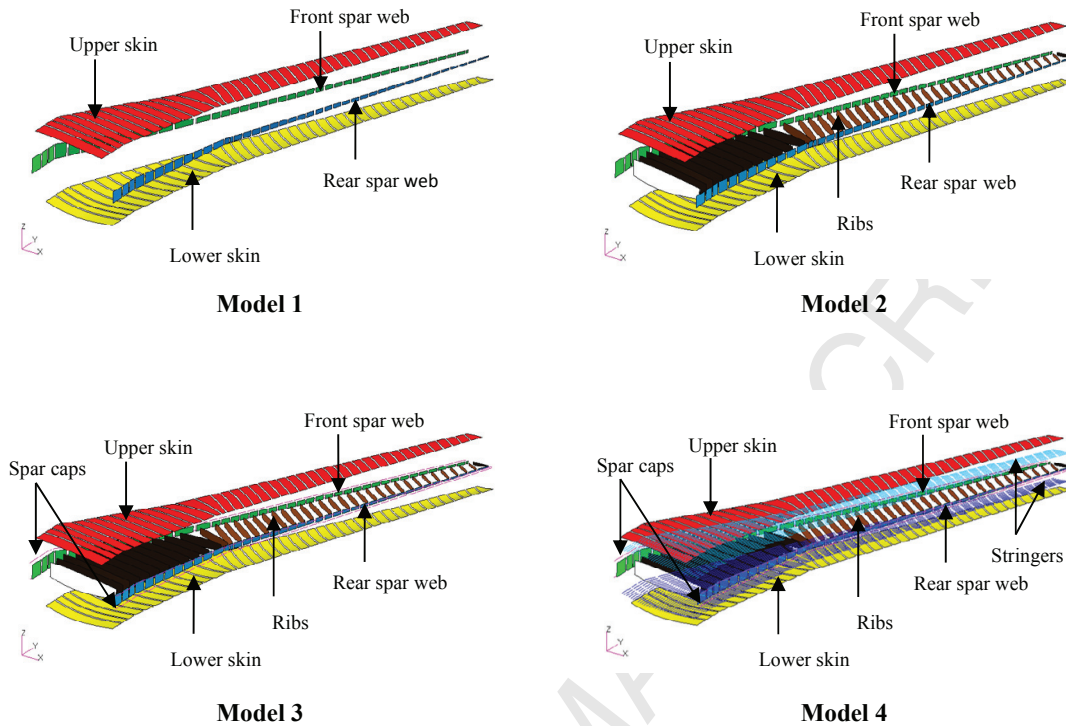
330

331

332

333

334

335

336

337

338

339

340

341

Fig. 11 Design optimization zones of CRM wingbox-Models 1-4

342 **4.2   Formulation of the CRM wingbox optimization problem**

343   During this study, it was decided to formulate this optimization problem in a simple way as possible,

344 in order to stay focused on the main objective and ensure a thorough understanding of the decisions made,

345 including how to solve or eliminate any unusual situations that may arise during the solution process. The

346 masses of the metallic and composite configurations of the CRM wingbox were minimized when

347 subjected to static strength/stiffness constraints on the design variables. The optimization problem

348 mathematically formulated in terms of the objective function, design variables and imposed constraints as

349 follows:

350 1. Objective function

351   The objective function is the structural mass of the CRM wingbox. The objective function can be

352 represented by:

$$\text{minimize } M(\boldsymbol{x}), \text{ where } M(\boldsymbol{x}) \text{ is the structural mass of the CRM wingbox} \qquad (1)$$

353 2. Design variables

354   For the optimization problem, considering the wingbox construction material to be a metallic material,

355 one design variable per design field is defined. The design variables include the thicknesses of the

356 wingbox skins, spar webs and ribs, as well as the cross-sectional areas of the wingbox spar caps and

357 stiffeners. A minimum gauge thickness of 2 mm and a cross-sectional area of 144 mm^2 are specified for
358 the design variables. The limits on the design variables are defined as follows:

$$2.0 \leq t_{metallic} \tag{2}$$

$$144.0 \leq a_{metallic} \tag{3}$$

359 On the other hand, considering the wingbox construction material to be a composite material, the
360 corresponding design variables for the wingbox skins, spar webs and ribs are the thicknesses of each ply
361 or lamina in the composite laminate associated with each design field. The cross-sectional areas of the
362 composite spar caps and stiffeners are also treated as individual design variables for each design zone.
363 The minimum ply thickness is taken to be 0.127 mm; while a 3 mm minimum gauge laminate thickness is
364 recommended to maintain an adequate level of laminate damage tolerance. The laminate ply thicknesses
365 are treated as individual design variables and a count is made of the required number of plies in each ply
366 orientation angle. The limits on the number of plies in each ply orientation angle are given as

$$3 \leq n_{ply} \tag{4}$$

367 Minimum cross-sectional areas of 216 mm^2 for the composite spar caps and stiffeners are specified
368 and the limits on the design variables are defined as

$$216.0 \leq a_{composite} \tag{5}$$

369 3. Static strength design constraints

370 For metallic skin panels, spar webs and ribs, the von Mises stress is checked against the material
371 allowable stress as defined in the following equation:

$$\sigma_{von\,Mises} \leq \sigma_{allowable} \tag{6}$$

372 For composite skin panels, spar webs and ribs, the Tsai-Wu criterion [42,43,44] is used to predict the
373 strength of the composite laminate in terms of the failure index (FI). For orthotropic plate analysis, under
374 the plane stress state, the Tsai-Wu strength theory predicts that a lamina will undergo failure when the
375 following inequality in satisfied:

$$FI = F_1\sigma_1 + F_2\sigma_2 + F_{11}\sigma_1^2 + 2F_{12}\sigma_1\sigma_2 + F_{22}\sigma_2^2 + F_{66}\sigma_6^2 \geq 1. \tag{7}$$

376 The coefficients F_1-F_{66}, with the exception of F_{12}, are described in terms of strengths in the principal
377 material directions. F_{12} accounts for the interaction between normal stresses, σ_1 and σ_2.

378 The principal strains in each ply are also checked against the material allowable strain to ensure the
379 integrity of the plies and failure-free laminates. The allowable strain value of $3500\,\mu\varepsilon$ includes the
380 margins due to fatigue and damage tolerance, assuming that the allowable strains are identical in terms of
381 tension and compression. Thus, the following constraint is placed on the strain value used for sizing the
382 structure:

$$\varepsilon_{principal} \leq \varepsilon_{allowable} \tag{8}$$

383   The spar caps and the longitudinal stiffeners are designed to carry axial stress only. Therefore, they

384   are designed according to their stress state against the allowable stress of the material as defined in the

385   following equation:

$$\sigma_{axial} \leq \sigma_{allowable} \qquad (9)$$

386   4. Static stiffness constraints

387   The flexural stiffness of the wingbox is controlled by limiting the vertical displacement of the wingtip

388   leading edge [45,46]. The wingtip deflection $\delta_{tip(Z)}$ for the CRM wing at a 2.5g pull-up maneuver is

389   assumed to be 15% of the wing semi-span b.

$$\delta_{tip(Z)} \leq 15\% \cdot b \qquad (10)$$

390   The torsional stiffness, which is necessary to counteract the twisting of the wing under aerodynamic

391   loads and thus prevents flutter, is controlled by constraining the twist angle at the tip chord of the wing.

392   The angular deformation at the wingtip chord is constrained by limiting it to a value of 6° to ensure

393   sufficient torsional stiffness and thus an adequate aeroelastic response [43]. The twist angle constraint is

394   defined using the vertical displacements at the wingtip chord ends. Equation (11) shows that the twist

395   angle at the wingtip should not exceed 6°. $(\delta)_{max}^{+}$ and $(\delta)_{max}^{-}$ are the maximum vertical displacements in

396   positive and negative directions of the z-coordinate, respectively. Here, C is the wing chord length at the

397   required location:

$$\Theta_{tip} \leq 6°, \text{ where } \Theta = \arctan\left(\frac{(\delta)_{max}^{+} - (\delta)_{max}^{-}}{C}\right) \qquad (11)$$

398   **4.3   Optimization results of the metallic and composite CRM wingbox models**

399   The CRM wingbox was optimized to meet static strength and stiffness requirements subject to lift

400   force only. In this initial study, no aeroelastic or manufacturing constraints are imposed nor any other

401   types of aerodynamic or inertial forces included, keeping the problem simple and focusing on the effects

402   of using different structural wingbox models for the structural optimization. Moreover, all the design

403   variables for this problem were treated as continuous design variables. The gradient-based optimization

404   algorithm, DOT, was used for the design sizing of the CRM metallic and composite wingbox models.

405   During this initial stage, it was decided to formulate this optimization study in a simple way as possible,

406   in order to stay focused on the main objective and ensure a thorough understanding of the decisions made,

407   including how to solve or eliminate any unusual situations that may arise during the solution process. In

408   the optimization process, the design variables change continuously within a range between a lower limit

409   and an unbounded upper limit. Therefore, the thicknesses and cross-sectional areas of the wingbox model

410   structural components are allowed to vary until all the design requirements are met. During the

411   optimization, convergence is aimed for by using different starting values for the design variables, and the

412   effects of these starting values on the final optimization are investigated. The sets of initial values for the

413   design variables, the thin panel thicknesses, the number of plies in each ply orientation and the flange

414 cross-sectional areas, for both the metallic and composite CRM wingbox optimization models, are
415 specified as follows:

$$t_{metallic} = \{2, 4, 6, 10, 13\} \text{ mm,} \tag{12}$$

$$n_{ply} = \{3, 4, 8, 11, 15\}, \tag{13}$$

$$a_{metallic} = \{144, 215, 420, 643, 858\} \text{ mm}^2, \tag{14}$$

$$a_{composite} = \{218, 258, 358, 585, 858\} \text{ mm}^2. \tag{15}$$

416 Tables 1 and 2 show the optimized masses of the metallic and composite CRM wingbox models,
417 respectively, using the sets of initial values for the design variables. Based on the results, it can be seen
418 that by using different initial guesses for the design variables, various local optimum designs can be
419 obtained from the gradient-based optimization solution. In all the solutions, convergence is achieved and
420 the bold values in the tables denote the local minimum solutions obtained for each CRM wingbox model.

421 **Table 1** Optimized masses of metallic CRM wingbox models (kg)

Design variables and initial values				
$t_1|a_1$	$t_2|a_2$	$t_3|a_3$	$t_4|a_4$	$t_5|a_5$
Wingbox Model 1				
17,990	18,587	18,641	18,531	17,999
Wingbox Model 2				
12,167	12,271	12,166	**12,149**	12,157
Wingbox Model 3				
12,245	12,129	12,167	12,276	**12,116**
Wingbox Model 4				
12,276	**12,272**	12,325	12,445	12,401

422

423 **Table 2** Optimized masses of composite CRM wingbox models (kg)

Design variables and initial values				
$\mathbf{n_{ply1}}|a_1$	$n_{ply2}|a_2$	$n_{ply3}|a_3$	$n_{ply4}|a_4$	$n_{ply5}|a_5$
Wingbox Model 1				
12,862	13,468	13,449	13,461	13,514
Wingbox Model 2				
8,535	9,070	9,355	**8,321**	8,587
Wingbox Model 3				
8,373	8,269	9,093	9,058	**7,891**
Wingbox Model 4				
8,917	7,940	**7,192**	8,367	7,366

424   The optimized masses of the second, third and fourth wingbox models; turned out to be lower than
425   those obtained by the use of the first wingbox model. Therefore, it can be seen that, in the context of using
426   high-fidelity structural models to describe and represent the CRM wingbox design, these models attempt
427   to improve the optimized masses of the wingbox. This representation of the CRM wingbox increases the
428   number of structural elements describing the wingbox from one model to the next. Thus, the number of
429   design variables increases and the design space becomes larger. The possible design alternatives within
430   the design domain thus increase, thereby increasing the chances of arriving at a better local optimum
431   solution and mass estimate.

432   The optimized masses of the composite wingbox models indicate that the results are more sensitive to
433   their initial starting values for the design variables than the results of the metallic wingbox models. In this
434   case, there is a greater difference in the optimized masses between the composite wingbox models than
435   for the metallic wingbox models. This behavior can be explained by the different mechanical properties
436   of the composite laminate, which are more complex than those of the metallic material. The global
437   laminate properties are dependent on the fiber orientation angles, the number of layers and their
438   thicknesses, and the stacking sequence. For an orthotropic material, at least two elastic constants are
439   needed to describe the stress-strain behavior in the material. Therefore, the stiffness of an orthotropic
440   plate must be described by two values, one along the longitudinal direction of the fibers, commonly
441   referred to as E_L, and one transverse to the direction of the fibers, usually denoted by E_T. Using classical
442   lamination theory [42,43,44], the bending stiffness matrix of the symmetric laminate $[\boldsymbol{D}]$ can be written
443   as

$$[\boldsymbol{D}] = \frac{2}{3} \sum_{k=1}^{n_{ply}} [\overline{\boldsymbol{Q}}]_K (Z_k^3 - Z_{k+1}^3), \qquad (16)$$

444   where $[\overline{\boldsymbol{Q}}]_K$ is the transformed reduced stiffness matrix of the kth layer, $(Z_k - Z_{k+1})$ is the ply thickness
445   and n_{ply} is the number of plies. The transformed reduced stiffness matrix can be defined in terms of the
446   ply angle ϕ and the elastic constants E_{11}, E_{22}, ν_{12} and G_{12} of the orthotropic layer. The mathematical
447   derivation of $[\overline{\boldsymbol{Q}}]_K$ can be found in [42,43]. On the other hand, the bending stiffness k_b of beam-like
448   metallic structures under an applied force F [48,49], as shown in Fig. 12, can be defined as

449

450

451

452

453
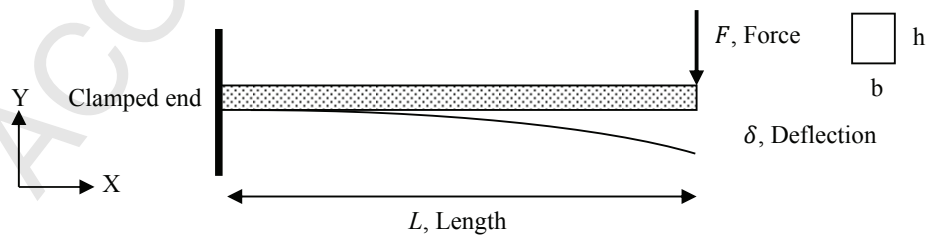
454   **Fig. 12** Deflection of cantilevered beam

$$k_b = \frac{F}{\delta} = \frac{3EI_{xx}}{L^3} \text{ , where } I_{xx} = \frac{1}{12}bh^3, E \text{ is Young}'s \text{ Modulus.} \qquad (17)$$

455   Mathematically, the area moment of inertia I_{xx} appears in the numerator of the stiffness equation,

456   Eqn. (17), therefore the larger the area moment of the inertia, the less the structure deflects and thus the

457   greater the stiffness. According to Eqns. (16) and (17), the derivation of the composite laminate bending

458   stiffness with respect to the layer thickness is a bit more complex than for the metallic isotropic material,

459   where the stiffness is described by one constant value; the modulus E of the material regardless of the

460   direction of load. An infinitesimal change in the composite layer thickness has an influence on its own

461   stiffness and on the stiffness of all the layers above. We can therefore create an equivalent design with the

462   same bending stiffness by changing the thicknesses of the composite layers while preserving the original

463   ply orientation of each layer and the same total thickness of the laminate. The existence of multiple

464   laminate equivalent designs has important implications for the optimization process, in that it results in

465   multiple optima and will always have a major influence on the objective function value.

466   The accuracy of the four proposed wingbox models in predicting the mass of the primary wing

467   structure is analyzed using the estimated optimum mass of the fourth wingbox model m_4 as a reference

468   value. Table 3 shows the errors of the wingbox masses predicted using the four different models of

469   increasing structural complexity. The error has been calculated as

470   **Table 3** Errors of the wingbox mass estimation

Wingbox Model	Metallic [%]	Composite [%]
Model 1	31.78	44.08
Model 2	-1.01	13.57
Model 3	-1.29	8.86
Model 4	0.00	0.00

471

472   From Table 3, it is observed that the first wingbox model over predicts the primary wing structure

473   mass for the CRM aircraft in comparison with the other models. A possible cause for this larger deviation

474   of Model 1 can be explained by the lack of internal chordwise oriented wing structural elements, meaning

475   that the wing skins have to carry an additional part of the lift load that is usually transferred to the wing

476   main spar by the ribs. Furthermore, the first wingbox model is a hollow beam and is less efficient than the

477   rest of the models, which contain ribs with hybrid orientation, in torsional stiffness. As a consequence, the

478   wingbox skin thicknesses are increased, resulting in an increase in the mass of the wingbox. From the

479   results summarized in Table 3, it can be seen that the second and third metallic wingbox models show

480   good accuracy with errors of -1.01 and -1.29%, respectively, for the mass estimation of the CRM

481   wingbox. For the composite wingbox models, this is not the case. The second and third composite

482   wingbox models over predict the primary wing structure mass for the CRM aircraft with errors of 13.57

483   and 8.86%, respectively.

484   The total wall-clock time for each optimization run until convergence occurs and an optimum solution

485   has been found is also compared, and the summary of the computational time is shown in Table 4. In this

486   study, computations were carried out on a laptop computer with a 2.60 GHz Intel i5 CPU and 8GB RAM.

487   From the results given in Table 4, it can be seen that the computational times for the optimized composite

488   models are very long compared to the optimized metallic models, as the design space for the composite

489   models is relatively complex with a large number of design variables and constraints. Furthermore, it is

490   also observed that the optimization run time was significantly increased for the fourth wingbox mass

491   estimation model for both the metallic and composite CRM wingbox configurations. Despite the long run

492   time, the fourth wingbox model is shown to have improved the accuracy of the objective function value,

493   particularly for the CRM composite wingbox model, as explained in the foregoing discussion of the

494   results presented in Table 3.

495   **Table 4** Total wall-clock time (seconds)

Wingbox Model	Metallic [s]	Composite [s]
Model 1	55.5	562.6
Model 2	55.9	497.1
Model 3	63.9	662.9
Model 4	742.4	5,303.4

496

497   The values of the CRM wingbox mass obtained in the current study are compared with the estimated

498   mass values according to the open scientific literature. It should be noted that no mass values were

499   reported for the composite CRM wingbox in the literature. Generally, the wingbox mass value of the

500   metallic CRM wing calculated in the current study is in good agreement with the value estimated

501   (12,263kg) by Kenway et al. [50]. On the other hand, the CRM wingbox mass (11,494 kg) calculated by

502   Klimmek [51] is lower than the mass reported in the current study. Possible sources for discrepancies can

503   be traced to the location of the spars and the number of ribs, as well as their spacing and location, which

504   have a direct effect on the wingbox mass. Flight conditions for the calculation of sizing loads and/or

505   aerodynamic loads, the definition and number of design variables and constraints in the scenario of using

506   optimization techniques.

507   **5. Concluding remarks**

508   Based on the results presented in Tables 1 and 2 in this study, the following points could be

509   concluded:

510   • In a scenario where high-fidelity structural models are used to describe and represent the CRM

511   wingbox model, these models do indeed attempt to improve the optimized masses of the wingbox.

512   This representation of the CRM wingbox increases the number of structural elements describing

513   the wingbox from one model to the next. Thus, the number of design variables increases, and the

514   design space enlarges. The possible design alternatives within the design domain then increase,

515   which in turn increases the chances of arriving at a better local optimum solution and mass

516   estimate.

517   • The mass of the metallic CRM wing box can be estimated with an acceptable level of accuracy and

518   reduced computational time with high degree of confidence by using the second wingbox model of

519   structural fidelity, as long as the gradient-based designs are also optimized using a sufficient

520   number of different starting values for the design variables, as practiced in the design and
521   optimization phase of this study (See Table 1).

522   • In the scenario where composite materials are used as the primary construction material for the
523   design of the CRM wingbox, it is observed that by increasing the structural fidelity of the wingbox
524   model, as observed in the second and third wingbox models, the discrepancy in the mass estimate
525   becomes smaller but still significant. Therefore, it is strongly recommended that the fourth
526   wingbox model be used as the baseline model for the preliminary estimate of the composite CRM
527   wingbox mass, requiring higher computational time in order to achieve the required accuracy
528   level.

529   • The optimized masses of the composite wingbox models indicate that the results are more
530   sensitive to the initial starting values of the design variables than to the results of the metallic
531   wingbox models (See Table 1 and 2). In this case, the change in the optimized masses of the
532   composite wingbox models is larger than the change for the metallic wingbox. This behavior can
533   be explained by the different mechanical properties of the composite laminate, which are more
534   complex than those of metallic structures. The computational times for the optimized composite
535   models are long and the design space is relatively complex, with a large number of design
536   variables and constraints compared to the optimized metallic models.

537   **6. Future work**

538   In the view of the above, and for a more detailed insight into the CRM wingbox mass estimation,
539   further studies that will account for the effects of considering aeroelasticity, buckling, fatigue and damage
540   tolerance, manufacturing requirements, and inertial forces will be considered using multidisciplinary
541   design optimization technique. This will aim to achieve a better understanding of the actual wingbox
542   structural material distributions in terms of thickness and orientation, and finally to assess the structural
543   behavior of the wing, including global displacement and local stresses. This will be a rather appropriate
544   view compared to that from an industrial design perspective.

545   **References**

546   [1]   Raymer, D. P. (2006). *Aircraft Design: A Conceptual Approach* (4th ed.). Washington, USA:
547   AIAA Education Series.

548   [2]   Roskam, J. (1989). *Airplane Design: Part III - Layout Design of Cockpit, Fuselage, Wing and
549   Empennage: Cutaways and Inboard Profiles.* Kansas: Roskam Aviation and Engineering
550   Corporation.

551   [3]   Torenbeek, E. (1982). *Synthesis of Subsonic Airplane Design.* Amsterdam: Delft University Press.

552   [4]   Ediger, K., Zeumer, C., & Dugas, M. (2004). *FAME-liA 4.00 F3 - Validation Document.* Technical
553   Report, Airbus Deutschland GmbH.

18

554 [5] Klimmek, T. (2014). Parametric Set-Up of a Structural Model for FERMAT Configuration for
555   Aeroelastic and Loads Analysis. *ASDJournal, 3,* (2), 31-49.

556 [6] Jutte, C. V., Stanford, B. K., & Wieseman, C. D. (2015). *Internal Structural Design of the*
557   *Common Research Model Wing Box for Aeroelastic Tailoring.* Hampton, Virginia: NASA.

558 [7] Murphy, N. (1987). *Analytical Wing Weight Prediction/Estimation Using Computer Based Design*
559   *Techniques.* PhD Thesis, Cranfield Institute of Technology.

560 [8] Ardema, M., Chambers, M., Patron, A., Hahn, A., Miura, H., & Moore, M. (1996). *Analytical*
561   *Fuselage and Wing Weight Estimation of Transport Aircraft.* NASA.

562 [9] Kundu, A. (2010). *Aircraft Design.* Cambridge: Cambridge University Press.

563 [10] Elham, A. (2013). *Weight Indexing for Multidisciplinary Design Optimization of Lifting Surfaces.*
564   PhD Thesis, Delft University of Technology.

565 [11] Howe, D. (2000). *Aircraft Conceptual Design Synthesis.* London: Professional Engineering
566   Publishing Limited London and Bury St Edmunds.

567 [12] Dababneh, O and Kipouros, T (2018). A review of aircraft wing mass estimation methods.
568   *Aerospace Science and Technology*, *72*, 256-266.

569 [13] Droegkamp, M. (1992). Finite Element Model Weight Estimation. SAWE Paper No. 2089, *51st*
570   *Annual Conference.* Hartford, Connnecticut: Society of Allied Weight Engineers, Inc.

571 [14] Zaidel, S. J. (1992). A-12 Structural Target Weight Distribution Using the Finite Element Model
572   (FEM). SAWE Paper No. 2110, *51st Annual Conference.* Hartford, Connnecticut: Society of
573   Allied Weight Engineers, Inc.

574 [15] Mitchell, P. M. (1993). Advanced Finite Element Weight Estimation Process on the High Speed
575   Civil Transport. SAWE Paper No. 2169, *52nd Annual Conference.* Biloxi, Mississippi: Society of
576   Allied Weight Engineers, Inc.

577 [16] Wenzel, J., Sinapius, U., & Gabbert, U. (2012). Primary Structure Mass Estimation in Early
578   Phases of Aircraft Development using the Finite Element Method. *CEAS Aeronautical Journal, 3*
579   (1), 35-44.

580 [17] Dababneh, O., & Kayran, A. (2014). Design, analysis and optimization of thin walled semi-
581   monocoque wing structures using different structural idealization in the preliminary design phase.
582   *International Journal of Structural Integrity*, *5* (3), 214-226.

583 [18] Bindolino, G., Ghiringhelli, G., Ricci, S., & Terraneo, M. (2010). Multilevel Structural
584   Optimization for Preliminary Wing-Box Weight. *Journal of Aircraft, 47, No. 2*, 475-489.

585 [19] Hurlimann, F., Kelm, R., Dugas, M., Oltmann, K., & Kress, G. (2010). Mass estimation of
586   transport aircraft wingbox structures with a CAD/CAE-based multidisciplinary process. *Aerospace*
587   *Science and Technology, 15* (4), 323-333.

588 [20] Dorbath, F., Nagel, B., & Gollnick, V. (2012). A Knowledge Based Approach for Extended
589   Physics-Based Wing Mass Estimation in early Design Stages. *28th Congress of the International*
590   *Council of the Aeronautical Sciences. 6.* Brisbane: ICAS.

591 [21] Holden, C. M., & Keane, A. J. (2004). Visualization Methodologies in Aircraft Design. AIAA-
592   2004-4449. *10th AIAA/ISSMO Multidisciplinary Analysis and Optimization Conference.* Albany,
593   New York.

594 [22] Ciampa, P. M., Nagel, B., & Tooren, M. (2010). Global Local Structural Optimization of
595   Transportation Aircraft Wings. AIAA 2010-3098. *51st AIAA/ASME/ASCE/AHS/ASC Structures,*
596   *Structural Dynamics, and Materials Conference.* Orlando, Florida: AIAA.

597 [23] Yang, Y., Wu, Z., & Yang, C. (2012). Equivalent Plate Modeling for Complex Wing
598   Configurations. *Procedia Engineering, 31,* 409-415.

599 [24] Ritter, M., & Cesnik, C. (2016). Large Deformation Modeling of a Beam Type Structure and a 3D
600   Wingbox using an Enhanced Modal Approach. AIAA 2016-1708. *57th*
601   *AIAA/ASME/ASCE/AHS/ASC Structures, Structural Dynamics, and Materials Conference.* San
602   Diego, California: AIAA.

603 [25] Werter, N., & Breuker, R. (2015). Aeroelastic tailoring and structural optimization using an
604   advanced dynamic aeroelastic framework. *IFASD 2015: 16th International Forum on*
605   *Aeroelasticity and Structural Dynamics Conference*. Saint Petersburg, Russia.

606 [26] EASA. (2015). *Certification Specifications and Acceptable Means of Compleance for Large*
607   *Aeroplanes CS-25, Amendment 16.* Retrieved March 28, 2015, from
608   http://easa.europa.eu/system/files/dfu/CS-25 20Amdendment 16.pdf

609 [27] FAA. *FAR 25, Airworthiness Standards: Transport Category Airplanes* (*Title 14 CFR Part 25*).
610   Retrieved January 15, 2014, from http://flightsimaviation.com/data/FARS/part_25.html

611 [28] ASM. (1978). *ASM Aerospace Specification Metals, Aluminum 7050-T7451*. Retrieved June 12,
612   2014, from http://asm.matweb.com/search/SpecificMaterial.asp?bassnum=MA7050T745

613 [29] ASM. (1978). *ASM Aerospace Specification Metals, Aluminum 2024-T3*. Retrieved June 12, 2014,
614   from http://asm.matweb.com/search/SpecificMaterial.asp?bassnum=%20MA2024T3

615 [30] Soni, S. R. (1980). *Elastic Properties of T300/5208 Bidirectional Symmetric Laminates -*
616   *Technical Report Afwal-Tr-80-4111.* Ohio 45433: Materials Laboratory - Air Force Wright
617   Aeronautical Laboratories - Air Force Systems Command.

618 [31] ESDU. (1999). *Computer program for estimation of spanwise loading of wings with camber and*
619   *twist in subsonic attached flow. Lifting-surface theory.* Retrieved March 12, 2014, from
620   https://www.esdu.com/cgi-bin/ps.pl?sess=cranfield5_1160220142018cql&t=doc&p=esdu_95010c

621 [32] Brennan, J. (1999). Integrating Optimization into the Design Process. *Proceedings of the Altair*
622   *HyperWorks Technology Showcase.* London.

623 [33] Cervellera, P. (2004). Optimization Driven Design Process: Practical Experience on Structural
624   Components. *Proceedings of the 14th Convegno Nazionae ADM.* Bari.

625 [34] Gartmeier, O., & Dunne, W. L. (1999). Structural Optimization in Vehicle Design Development.
626   *MSC. Worldwide Automotive Conference.*

627 [35] Krog, L., Tucker, A., & Rollema, G. (2002). Application of Topology, Sizing and Shape
628   Optimization Methods to Optimal Design of Aircraft Components. *3rd Altair UK HyperWorks*
629   *Users Conference.*

630 [36] Krog, L., Tucker, A., Kempt, M., & Boyd, R. (2004). Topology Optimization of Aircraft Wing
631   Box Ribs, AIAA-2004-4481. *Proc. 10th AIAA/ISSMO Symposium on Multidisciplinary Analysis*
632   *and Optimization.* Albany, NY.

633 [37] Schumacher, G., Stettner, M., Zotemantel, R., O'Leary, O., & Wagner, M. (2004). Optimization
634   Assisted Strcutural Design of New Military Transport Aircraft, AIAA-2004-4641. *Proc. 10th*
635   *AIAA MAO Conference.* Albany, NY.

636 [38] Venkayya, V. B. (1971). Design of Optimum Strcutures. *Computers and Structures* (No.1), 265-
637   309.

638 [39] Wang, Z., Huang, W. & Yan, L. (2014). Multidisciplinary design optimization approach and its
639   application to aerospace engineering. *Chinese Science Bulletin*, 59, (36), 5338-5353

640 [40] MSC Nastran (2012). *Design Sensitivity and Optimization User's Guide.* Santa Ana, CA:
641   MSC.Software Corporation.

642 [41] Dababneh O, Kipouros T & Whidborne JF (2018). Application of an efficient gradient-based
643   optimization strategy for aircraft wing structures, *Aerospace*, *5*, (1), 1-27.

644 [42] Jones, R. M. (1999). *Mechanics of Composite Materials* (2nd ed.). Taylor & Francis.

645 [43] Tsai, S. W., & Hahn, H. T. (1980). *Introduction to Composite Materials.* Technomic Publishing
646   Co.

647 [44] Kassapoglou, C. (2013). *Review of Laminate Strength and Failure Criteria, in Design and*
648   *Analysis of Composite Structures: With Applications to Aerospace Structures.* Oxford: John Wiley
649   & Sons Ltd.

650 [45] Starnes Jr, J. R., & Haftka, R. T. (1979). Preliminary Design of Composite Wings for Buckling,
651   Stress and Displacement Constraints. *Journal of Aircraft, 16* (8), 564-570.

652 [46] Oliver, M., climent, H., & Rosich, F. (1999). Non Linear Effects of Applied Loads and Large
653   Deformations on Aircraft Normal Modes. *RTO AVT Specialists' Meeting on Strucrural Aspects of*
654   *Flexible Aircraft Control.* Ottawa.

655 [47] Liu, Q., Mulani, S., & Kapani, R. K. (2014). Global/Local Multidisciplinary Design Optimization
656   of Subsonic Wing, AIAA 2014-0471. *10th AIAA Multidisciplinary Design Optimization*
657   *Conference - AIAA SciTech.* National Harbor, Maryland: AIAA, Inc.

658 [48] Niu, M. C. (1999). *Airframe Stress Analysis and Sizing.* Conmilit Pres Ltd.

659 [49] Beer, F., Johnston, J. E., DeWolf, J., & Mazurek, D. (2014). *Mechanics of Materials* (7th ed.).
660   McGraw-Hill Education.

661 [50] Kenway, G. K., Martins, J. R., & Kennedy, G. J. (2014). Aerostructural optimization of the
662   Common Research Model configuration, AIAA 2014-3274. *15th AIAA/ISSMO Multidisciplinary*
663   *Analysis and Optimization Conference.* Atlanta, GA: AIAA Aviation.

664 [51] Klimmek, T. (2014). Parametric Set-Up of a Structural Model for FERMAT Configuration for
665   Aeroelastic and Loads Analysis. *ASDJournal, 3, (2), 31-49.*

Influence of high fidelity structural models on the predicted mass of aircraft wing using design optimization

Dababneh, Odeh